Liquid Structure of Room-Temperature Ionic Liquid, 1-Ethyl-3-methylimidazolium Bis-(trifluoromethanesulfonyl) Imide

ARTICLE *in* THE JOURNAL OF PHYSICAL CHEMISTRY B · MAY 2008

Impact Factor: 3.3 · DOI: 10.1021/jp7105499 · Source: PubMed

Liquid Structure of Room-Temperature Ionic Liquid, 1-Ethyl-3-methylimidazolium Bis-(trifluoromethanesulfonyl) Imide

Kenta Fujii,[†] Yasufumi Soejima,[†] Yasuhiro Kyoshoin,[†] Shuhei Fukuda,[‡] Ryo Kanzaki,[‡] Yasuhiro Umebayashi,[‡] Toshio Yamaguchi,[§] Shin-ichi Ishiguro,*[,‡] and Toshiyuki Takamuku*[,†]

Department of Chemistry and Applied Chemistry, Faculty of Science and Engineering, Saga University, Honjo-machi, Saga 840-8502, Japan, Department of Chemistry, Faculty of Science, Kyushu University, Hakozaki, Higashi-ku, Fukuoka 812-8581, Japan, and Advanced Materials Institute and Department of Chemistry, Faculty of Science, Fukuoka University, Nanakuma, Jonan-ku, Fukuoka 814-0180, Japan

Received: November 1, 2007; In Final Form: January 19, 2008

The liquid structure of 1-ethyl-3-methylimidazolium bis-(trifluoromethanesulfonyl) imide (EMI^+TFSI^-) has been studied by means of large-angle X-ray scattering (LAXS), ^1H, ^{13}C, and ^{19}F NMR, and molecular dynamics (MD) simulations. LAXS measurements show that the ionic liquid is highly structured with intermolecular interactions at around 6, 9, and 15 Å. The intermolecular interactions at around 6, 9, and 15 Å are ascribed, on the basis of the MD simulation, to the nearest neighbor $EMI^+\cdots TFSI^-$ interaction, the $EMI^+\cdots EMI^+$ and $TFSI^-\cdots TFSI^-$ interactions, and the second neighbor $EMI^+\cdots TFSI^-$ interaction, respectively. The ionic liquid involves two conformers, C_1 (cis) and C_2 (trans), for $TFSI^-$, and two conformers, planar cis and nonplanar staggered, for EMI^+, and thus the system involves four types of the $EMI^+\cdots TFSI^-$ interactions in the liquid state by taking into account the conformers. However, the $EMI^+\cdots TFSI^-$ interaction is not largely different for all combinations of the conformers. The same applies also to the $EMI^+\cdots EMI^+$ and $TFSI^-\cdots TFSI^-$ interactions. It is suggested from the ^{13}C NMR that the imidazolium C2 proton of EMI^+ strongly interacts with the O atom of the $-SO_2(CF_3)$ group of $TFSI^-$. The interaction is not ascribed to hydrogen-bonding, according to the MD simulation. It is shown that the liquid structure is significantly different from the layered crystal structure that involves only the nonplanar staggered EMI^+ and C_1 $TFSI^-$ conformers.

Introduction

Nonvolatile and incombustible room-temperature ionic liquids (RTILs) are considered to be green solvents for lithium secondary batteries.[1−4] The usage of these RTILs extensively spreads into various field of application in recent years, but basic studies on their physicochemical properties, particularly the liquid structure, are limited. It has been established that metal−ion complexation in solution strongly depends on the liquid structure or the solvent−solvent interaction of the solvent.[5] The same may also apply to the RTILs as the solvent, but our knowledge on the liquid structure of RTILs is limited at the present stage.

A few structural studies have so far been reported for RTILs consisting of 1-alkyl-3-methylimidazolium and bis-(trifluoromethanesulfonyl) imide ($TFSI^-$) ions by molecular dynamics (MD) simulation.[6] Takahashi et al. reported the liquid structure of 1-ethyl-3-methylimidazolium (EMI^+) tetrachloroaluminate by neutron diffraction measurement, which is the first direct approach to the liquid structure of RTILs.[7] A large-angle X-ray scattering (LAXS) study has been reported by Nishikawa et al. for the 1-butyl-3-methylimidazolium iodide, indicating the presence of a long-range ordering among iodide ions.[8] We pointed out that the EMI^+TFSI^- involves the C_1 and C_2 conformers of the anion in equilibrium, with the enthalpy of 3.5 kJ mol^{-1} for conformational change from C_2 to C_1, and that the dipole moment (4.4 D) of the C_1 is significantly lager than that (0.3 D) of the C_2.[9] Deetlefs et al. have reported the liquid structure of 1,3-dimethylimidazolium (DMI^+) $TFSI^-$ studied by large-angle neutron scattering (LANS) and revealed that the $TFSI^-$ ion is located over the imidazolium ring plane and also involves the C_1 and C_2 conformers.[10] These conformers are also present in crystals of DMI^+TFSI^- and 1,2,3-triethylimidazolium (TMI^+) $TFSI^-$.[11]

On the other hand, we found that the EMI^+X^- ($X^- = BF_4^-$, PF_6^-, $CF_3SO_3^-$, and $TFSI^-$) RTILs involve two conformers of the cation, the planar cis and nonplanar staggered conformers, in equilibrium.[12] However, no ion−ion interaction has been revealed for these RTILs yet. The crystal structure of EMI^+TFSI^- has been reported very recently, according to Choudhury et al.[13] The crystal involves the sole C_1 conformer of $TFSI^-$, and the $-SO_2-$ moieties are located on a plane involving imidazolium rings to form the $-CH\cdots O$ hydrogen bonds through the C2, C4, and C5 protons, although weak. The hydrogen-bonded network among the ions yields another plane involving the $-CF_3$ groups located out of the imidazolium-ring plane. Two planes of the $-CF_3$ groups are so arranged to interact with each other, at the $F\cdots F$ distance of 2.79−2.91 Å, to give a layered structure that is offset in an ABAB... type arrangement with distances of 5.3 and 8.1 Å between the centroids of the imidazolium rings of the adjacent layers. Thus, the liquid structure of EMI^+TFSI^- may be particularly interesting, because both ions involve conformers, and particularly, the dipole moment of the C_1 and C_2 conformers of the $TFSI^-$ ion are largely different.[9] The different ion−dipole interactions of the C_1 and C_2 conformers might lead to a different local distribution of the conformers

* To whom correspondence should be addressed. E-mail: analsscc@mbox.nc.kyushu-u.ac.jp (S.I.) and takamut@cc.saga-u.ac.jp (T.T.).
[†] Saga University.
[‡] Kyushu University.
[§] Fukuoka University.

10.1021/jp7105499 CCC: $40.75
Published on Web 03/19/2008

around the EMI^+ ion, or vise versa. However, no information on the local structure around each conformer is reported yet.

In the present work, the liquid structure of EMI^+TFSI^- at 298 K has thus been studied on the basis of LAXS measurement and MD simulation. In the MD simulation, the rigid model is employed for molecular structures of the conformers of EMI^+ and $TFSI^-$, in order to extract the specific local structure around each conformer. Based on the results of the LAXS and MD simulation, a plausible structure model will be proposed for the EMI^+TFSI^- RTIL. Interaction between EMI^+ and $TFSI^-$ ions is also examined by ^1H, ^{13}C and ^{19}F NMR over a range of temperature 313−263 K above the melting point (247 K).[13]

Experimental Section

Materials. EMI^+TFSI^- (Nippon Synthetic Chemical Industry) was used without further purification. Water content of EMI^+TFSI^- was estimated to be less than 100 ppm by a Karl Fischer titration. Density of EMI^+TFSI^- was measured using an electronic densimeter (Kyoto Electronics, DA-310) at 298.15 K.

LAXS Measurement. LAXS measurements for EMI^+TFSI^- were carried out using a rapid liquid X-ray diffractometer (BRUKER AXS, model DIP301) with an imaging plate (IP) (Fuji Film Co.). The Mo Kα radiation (the wavelength λ = 0.7107 Å) was generated from a rotary molybdenum anode (Rigaku, model RU-300) at 50 kV and 200 mA, and monochromatized using a flat graphite crystal. Details of the diffractometer have been described elsewhere.[14,15] A sample was sealed in a glass capillary (W. Müller Co.) of 2 mm inner diameter (0.01 mm wall thickness). The glass capillary without a sample was also measured for a background correction. Two-dimensional X-ray intensities $I_{obs}(x,y)$, where x and y are horizontal and vertical coordinates of an IP, were measured over the range 0.2°−109° of the scattering angle (2θ), which corresponds to the scattering vector s ($=4\pi\lambda^{-1}\sin\theta$) of 0.03−14.4 $Å^{-1}$. Data were accumulated for 1 h.

Observed intensities $I_{obs}(x,y)$ were integrated into one-dimensional $I_{obs}(\theta)$.[15] The intensities thus obtained were corrected for back ground, absorption, polarization and incoherent scatterings by the conventional methods to obtain coherent scatterings $I_{coh}(s)$.[16−19] The structure function $i(s)$ and radial distribution function (RDF) per stoichiometric volume containing a pair of EMI^+ and $TFSI^-$ ions $D(r)$ were obtained by

$$i(s) = \frac{I_{coh}(s) - \sum n_i f_i(s)^2}{(\sum n_i f_i(s))^2} \quad (1)$$

$$D(r) - 4\pi r^2 \rho_0 = \frac{2r}{\pi}\int_0^s si(s)\sin(rs)\exp(-Bs^2)\,ds \quad (2)$$

where n_i and $f_i(s)$ denote the number and the atomic scattering factor of atom i, respectively,[20] and ρ_0 is the number density, and B is the damping factor (0.01 $Å^2$ in this work). The structural parameters were obtained by analyzing $i(s)$ using program KURVLR.[21]

MD Simulation. An MD simulation for an *NTP* ensemble of 256 pairs of EMI^+ and $TFSI^-$ ions in a cubic cell at 298 K and 1 atm was carried out using the Materials Explorer 3.0 program package (Fujitsu). The simulation time was 2000 ps with a step of 1 fs. It took 1000 ps for the system to reach equilibrium, and data obtained in the range of 1000−2000 ps were used to calculate the partial radial distribution function $g(r)$. Lennard-Jones (LJ) and Coulomb terms were taken into account for intermolecular interactions. The LJ parameters employed here are those established by Lopes et al.,[22,23] and the coulomb parameters are listed in Table S1 (Supporting Information), which were evaluated according to the ChelpG method based on an MP2/cc-pVTZ(-f) calculation. In the calculation, the rigid model was employed for molecular structures of the planar cis and nonplanar staggered conformers of EMI^+ and the C_2 and C_1 conformers of $TFSI^-$.[9,12] Here, we assumed the 1:1 mixture of the conformers for each of EMI^+ and $TFSI^-$ ions. The simulated density of the EMI^+TFSI^- RTIL was 1.526 ± 0.002 g cm^{-3}, which is in good agreement with the experimental one (1.517 g cm^{-3}) measured at 298.15 K.

On the basis of the $g(r)$ obtained from the MD results, the structure function, $i(s)$ was calculated as

$$\begin{cases} i(s) = \dfrac{\sum_i \sum_j \{n_i(n_j - 1)f_i(s)f_j(s)/N(N-1)\}}{\{\sum_k (n_k f_k(s)/N)\}^2} \times \\ \quad \int_0^r 4\pi r^2 \rho_0 (g_{ij}(r) - 1)\dfrac{\sin(sr)}{sr}\,dr \;(i = j) \\ i(s) = \dfrac{\sum_i \sum_j (2n_i n_j f_i(s)f_j(s)/N^2)}{\{\sum_k (n_k f_k(s)/N)\}^2} \times \\ \quad \int_0^r 4\pi r^2 \rho_0 (g_{ij}(r) - 1)\dfrac{\sin(sr)}{sr}\,dr \;(i \neq j) \end{cases} \quad (3)$$

where ρ_0 denotes the average number density, and the total number of atoms in the cell N is given by

$$N = \sum_k n_k \quad (4)$$

The theoretical RDF was obtained by Fourier transform of the structure function thus calculated, and was compared with that observed by LAXS experiments.

NMR Spectroscopy. ^1H, ^{13}C, and ^{19}F NMR for EMI^+TFSI^- have been measured using an FT-NMR spectrometer (JEOL, JNM-AL300) over a range of temperatures, 313−263 K. The temperature of the sample chamber was kept constant during the measurements by flowing air passing through liquid nitrogen. The resolution was ±0.0012, ±0.017, and ±0.0013 ppm for ^1H, ^{13}C, and ^{19}F NMR, respectively. An external double reference tube (a capillary with a blown-up sphere at the end) was inserted into the sample tube (Shigemi, PS-001 super precision). Hexamethyldisiloxane (HMDS) was used as a reference substance for ^1H and ^{13}C, and trifluoromethylbenzene (TFMB) for ^{19}F. The observed chemical shifts were corrected for the volume magnetic susceptibility of EMI^+TFSI^- on the basis of an external double reference method as described below.[24−26] A couple of NMR signals with the chemical shift $\Delta\delta_{ref}$/ppm is obtained for a given reference substance. The chemical shift is related to the volume magnetic susceptibility of the sample liquid χ_s and the reference substance χ_r, as

$$\Delta\delta_{ref} = \kappa(\chi_s - \chi_r) \times 10^6 \quad (5)$$

where κ denotes the shape factor for the reference tube. The κ value has been determined in advance of sample measurements from the $\Delta\delta_{ref}$ data for $CDCl_3$, $(CD_3)_2SO$, C_6D_{12}, C_6D_6, and $(CD_3)_2CO$ measured at 298 K, as the χ_s values of which are

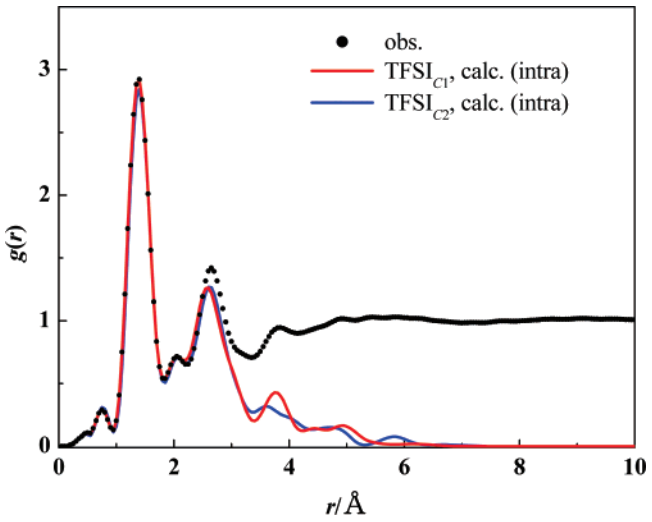

Figure 1. Observed $g(r)$ (the dotted line) and intramolecular $g_{intra}(r)$s calculated for EMI^+TFSI^- by taking into account their conformation, i.e., the EMI^+ and C_1 $TFSI^-$ conformers (the bold red line), and EMI^+ and C_2 $TFSI^-$ conformers (the bold blue line).

available from the literature.[24] The observed chemical shift δ_{obs} is corrected for the diamagnetic effect as

$$\delta_{corr} = \delta_{obs} - (4\pi/3)(\chi_s - \chi_r) \times 10^6 = \delta_{obs} - (4\pi/3\kappa)\Delta\delta_{ref} \quad (6)$$

where the δ_{obs} value is the shift from the reference signal in a capillary.

The δ_{corr} is further corrected for the volume change with temperature. The corrected chemical shift $\delta^{Tr}_{corr}(T)$ at a given temperature T is given as

$$\delta^{Tr}_{corr}(T) = \delta_{corr}(T) - (4\pi/3)\{(\chi_r(T) - \chi_r(T_r))\} \times 10^6 \quad (7)$$

where T_r represents the reference temperature (298 K in this work).[27] The value of $\chi_r(T_r)$ for HMDS is available from ref 24, and the value for TFMB was calculated using the mass magnetic susceptibility and the density.[27] The ^1H, ^{13}C, and ^{19}F NMR chemical shifts obtained at various temperature were thus normalized at 298 K.

Results and Discussion

LAXS. The observed radial distribution function (RDF) in the form of $g(r)$ is shown in Figure 1 (the dotted line), which is obtained by Fourier transform of the structure function $i(s)$. The observed $g(r)$ is the sum of intra- and intermolecular $g(r)$s, i.e., $g(r) = g_{intra}(r) + g_{inter}(r)$, and the $g_{intra}(r)$ can separately be evaluated by knowing molecular structures of EMI^+ and $TFSI^-$ ions, and by assuming appropriate temperature factors. As shown in Chart 1, the EMI^+TFSI^- RTIL involves conformers, i.e., the planar cis and nonplanar staggered conformers for EMI^+,[12] and the C_1 and C_2 conformers for $TFSI^-$.[9] The intramolecular RDFs of these conformers were evaluated by knowing respective structures in crystals, i.e., the planar cis and nonplanar staggered conformers of EMI^+ in the $EMI^+(HF_2)^-$ and EMI^+TFSI^- crystals,[13,28] and the C_1 and C_2 conformers of $TFSI^-$ in the EMI^+TFSI^- and *N*-butyl-*N*-methylpyrrolidinium (BMP^+) $TFSI^-$ crystals.[13,29] The intramolecular RDFs for the EMI^+ conformers thus evaluated are practically the same. On the other hand, the $TFSI^-$ conformers with the S2−N1−S9−C12 and S9−N1−S2−C5 dihedral angles of +112.9° and −84.3° (C_1) and 85.5° and 89.3° (C_2) show significantly different $g_{intra}(r)$s, which is ascribed mainly to the $CF_3\cdots CF_3$ interaction. The $g_{intra}(r)$s of the RTIL composed of the EMI^+ and C_1 $TFSI^-$ conformers (the red line), and the EMI^+ and C_2 $TFSI^-$ conformers (the blue line) are shown in Figure 1. The observed peaks in the range $r < 2.7$ Å are ascribed to the intramolecular interactions, i.e., the C−C, C−N, and N−S bonds at 1.4 Å, the nonbonding interactions within the imidazolium ring C···C, C···N, and N···N at 2.0 Å, and the nonbonding S···S interaction at 2.7 Å. In the range of 3−6 Å, the observed peak at 3.7 Å may mainly be ascribed to the intramolecular nonbonding $-SO\cdots CF_3$ interaction, although the calculated $g_{intra}(r)$s show significantly

CHART 1: Geometries of the C_1 and C_2 Conformers of $TFSI^-$ and the Nonplanar Staggered and Planar cis Conformers of EMI^+

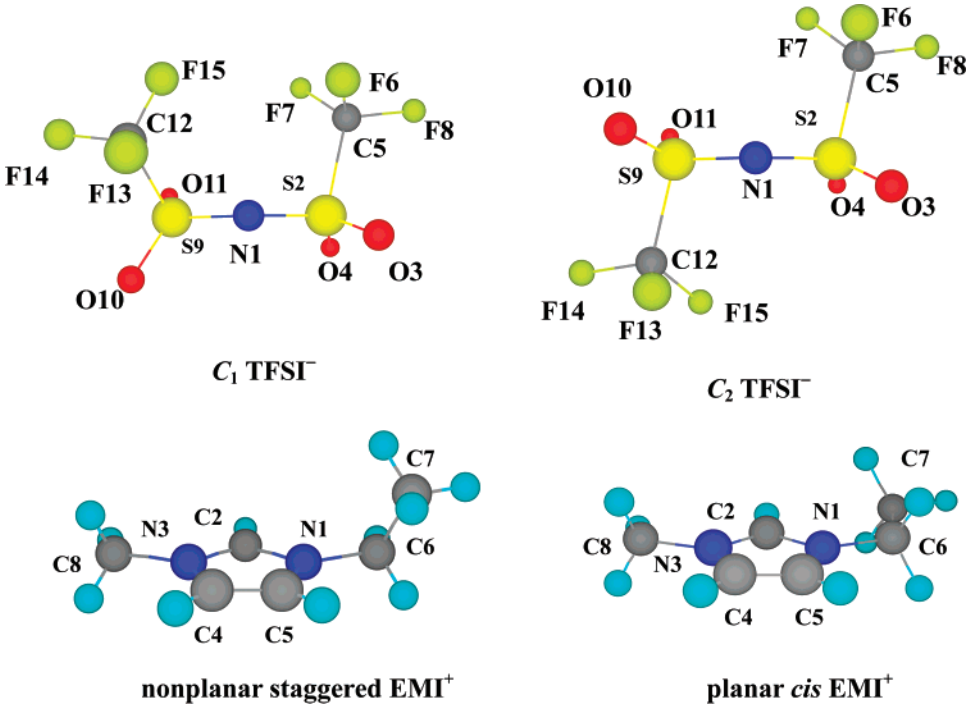

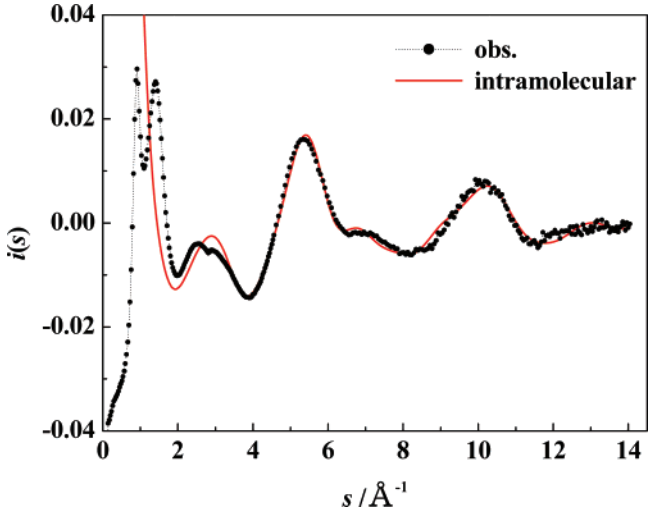

Figure 2. Observed structure function $i(s)$ (the dotted line) of the EMI^+TFSI^- RTIL at 298 K, and the intramolecular $i(s)$ for the RTIL involving 1:1 mixtures of the conformers (the red line).

different profiles depending on the conformer, and intra- and intermolecular interactions are overlapped. The nonbonding $CF_3\cdots CF_3$ interaction (4.7 Å) within the C_1 conformer and the $-CH_3\cdots C_2H_5$ interaction within the EMI^+ ion (4.7 Å), as well as the $-CF_3\cdots CF_3$ interaction within the C_2 conformer (5.7 Å), are not clearly identified in the observed $g(r)$. According to Choudhury et al.,[13] the intermolecular $-CF_3\cdots CF_3$ interaction appears at around 3.0 Å in the EMI^+TFSI^- crystal. The corresponding interaction is not seen in the observed $g(r)$, implying that the interaction is almost destroyed in the RTIL.

The $g_{inter}(r)$ can be obtained by subtracting the calculated $g_{intra}(r)$ from the observed $g(r)$. Evidently, the $g_{inter}(r)$ depends on the distribution of conformers, which is not known yet. According to our previous work on the bis(fluorosulfonyl) imide (FSI^-, $\{FS(O_2)\}_2N^-$) ion in EMI^+FSI^-[30] the FSI^- ion involves the C_1 and C_2 conformers like the $TFSI^-$ ion, and the enthalpy and entropy for the conformational change almost compensate with each other to give the corresponding Gibbs energy close to zero. Therefore, in the present work, we assume the 1:1 mixture of the conformers for both EMI^+ and $TFSI^-$ ions. The $i(s)$ for the intramolecular interaction of EMI^+TFSI^- thus calculated by assuming the 1:1 mixture is shown in Figure 2 (the red line), together with the observed $i(s)$ (the dotted line). The calculated $i(s)$ reproduces well the observed $i(s)$ over the range $s/Å^{-1} > 4$, indicating that the assumption may be valid as the first approximation. The difference between calculated and observed $i(s)$s in the range $s/Å^{-1} < 4$ indicates the presence of significant intermolecular interactions. However, the $g_{inter}(r)$ thus extracted is complicated with small peaks and shoulders over the whole range, and it is thus difficult to ascribe the observations to specific $EMI^+\cdots TFSI^-$, $EMI^+\cdots EMI^+$, and $TFSI^-\cdots TFSI^-$ interactions without the aid of theoretical calculations.

MD Simulation. The calculated system involves 256 ion-pairs of EMI^+ and $TFSI^-$, both of which are the 1:1 mixture of their conformers. The system thus involves four types of the $EMI^+\cdots TFSI^-$ interactions, i.e., the nonplanar staggered$\cdots C_1$ (type $i = 1$), nonplanar staggered$\cdots C_2$ (2), planar cis$\cdots C_1$ (3), and planar cis$\cdots C_2$ (4) interactions, and the individual $g_i^{EMI-TFSI}(r)$ ($i = 1-4$) are extracted on the basis of atom−atom correlations, Figure 3. As seen, although the dipole moment of the C_1 conformer is significantly larger than that of the C_2 conformer,[9] the profiles of the $g_i^{EMI-TFSI}(r)$ are similar for all types of ion pairs over the whole range. The $g_i^{EMI-TFSI}(r)$s show a shoulder

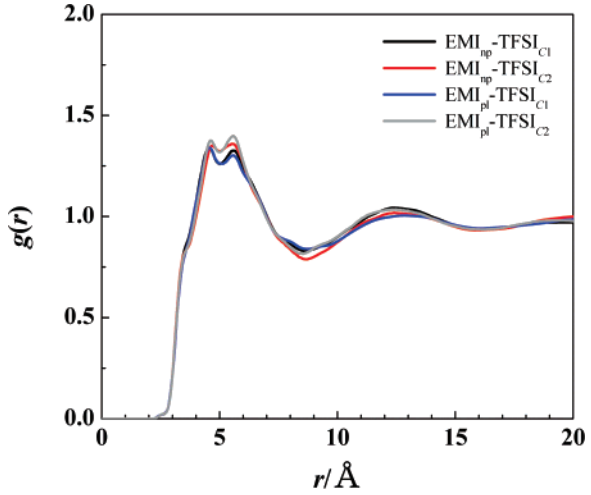

Figure 3. $g_i^{EMI-TFSI}(r)$s for EMI^+(nonplanar staggered)$\cdots TFSI^-(C_1)$, EMI^+(nonplanar staggered)$\cdots TFSI^-(C_2)$, EMI^+(planar cis)$\cdots TFSI^-(C_1)$, and EMI^+(planar cis)$\cdots TFSI^-(C_2)$ interactions.

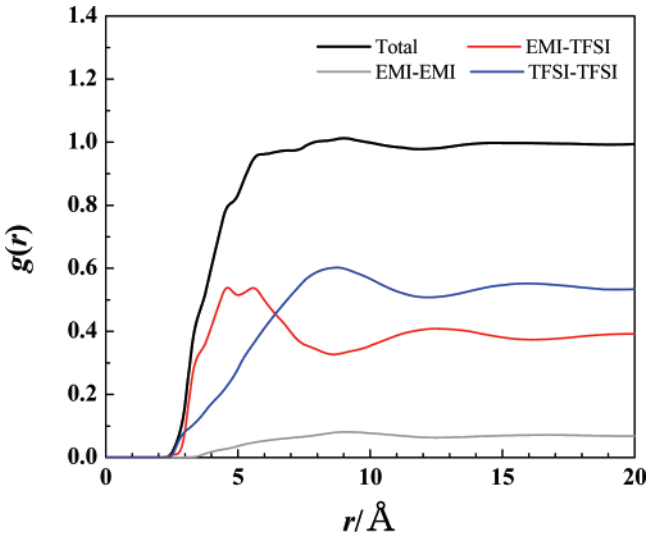

Figure 4. Partial $g^{EMI-TFSI}(r)$, $g^{EMI-EMI}(r)$, and $g^{TFSI-TFSI}(r)$ and their total sum $g(r)$, corrected for the atomic scattering factors.

at around 3.5 Å and peaks at around 4.6 and 5.7 Å for the contact ion pairs. The peak at 5.7 Å is even slightly higher for the C_2 conformer, implying that the dipole moment hardly plays an essential role in the contact ion-pair interactions. The detailed atom−atom correlations for the $EMI^+\cdots TFSI^-$ interactions will be discussed in a latter section. Similarly, the system involves three types of the $EMI^+\cdots EMI^+$ interactions, i.e., the nonplanar staggered$\cdots$nonplanar staggered ($i = 1$), nonplanar staggered$\cdots$planar cis (2), and planar cis$\cdots$planar cis (3) interactions, and three types of the $TFSI^-\cdots TFSI^-$ interactions, i.e., the $C_1\cdots C_1$ (1), $C_1\cdots C_2$ (2), and $C_2\cdots C_2$ (3) interactions. The $g_i^{EMI-EMI}(r)$ ($i = 1-3$) and $g_i^{TFSI-TFSI}(r)$ ($i = 1-3$) are given in Figure S1. Similar profiles of $g_i^{EMI-EMI}(r)$s, as well as $g_i^{TFSI-TFSI}(r)$s also obtained among all sets of conformers.

The partial radial distribution function $g(r)$s for the $EMI^+\cdots TFSI^-$, $EMI^+\cdots EMI^+$, and $TFSI^-\cdots TFSI^-$ interactions are calculated as $g^{EMI-TFSI}(r) = \Sigma_i g_i^{EMI-TFSI}(r)$ ($i = 1-4$), $g^{EMI-EMI}(r) = \Sigma_i g_i^{EMI-EMI}(r)$ ($i = 1-3$), and $g^{TFSI-TFSI}(r) = \Sigma_i g_i^{TFSI-TFSI}(r)$ ($i = 1-3$). The overall $g^{EMI-TFSI}(r)$, $g^{EMI-EMI}(r)$ and $g^{TFSI-TFSI}(r)$, together with the total $g_{inter}(r)$ $\{= g^{EMI-TFSI}(r) + g^{EMI-EMI}(r) + g^{TFSI-TFSI}(r)\}$, are shown in Figure 4, which are corrected for the atomic scattering factors to compare the calculated RDF with the observed one in the latter section. As

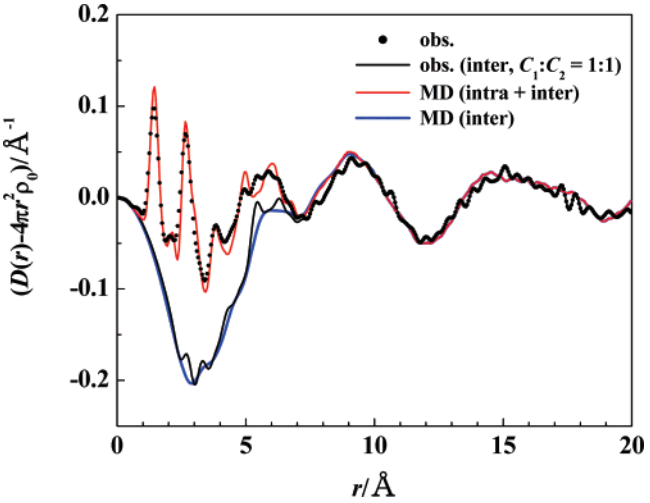

Figure 5. Observed (the dotted line) and calculated (the red line) RDFs of the EMI^+TFSI^- RTIL in the form of $D(r) - 4\pi r^2\rho_0$, and corresponding extracted (the black line) and calculated (the blue line) intermolecular RDFs.

seen, the contribution of the $g^{EMI-EMI}(r)$ is small relative to the $g^{EMI-TFSI}(r)$ and $g^{TFSI-TFSI}(r)$ over the whole range. The $g^{EMI-TFSI}(r)$ shows a valley at around 9 Å, i.e., the layered $EMI^+\cdots TFSI^-$ interaction found at around 8 Å in the EMI^+TFSI^- crystals[13] disappears in the RTIL, suggesting that the crystal structure is completely destroyed in the RTIL at 298 K. The second neighbor $EMI^+\cdots TFSI^-$ interaction appears at around 12 Å. On the other hand, the first neighbor $TFSI^-\cdots TFSI^-$ and $EMI^+\cdots EMI^+$ contacts occur at around 9 Å. The $g^{EMI-TFSI}(r)$ and $g^{TFSI-TFSI}(r)$ are strongly compensated to give the total $g_{inter}(r)$ with broad peaks and valleys at $r > 7$ Å, which is in parallel with the observed $g(r)$.

Intermolecular interactions can be described with emphasis using the RDF in the form of $D(r) = 4\pi r^2\rho_0 g(r)$, and the observed $D(r) - 4\pi r^2\rho_0$ (the dotted line) is shown in Figure 5, together with that calculated by the MD simulation (the red line). The calculated curve satisfactorily reproduces the observed one over the whole range $r < 20$ Å. The extracted intermolecular $D(r) - 4\pi r^2\rho_0$ (the solid line) is also depicted and compared with that calculated by the MD simulation (the blue line). The former was obtained by subtracting the intramolecular interaction for the 1:1 mixtures of the EMI^+ and $TFSI^-$ conformers, which is calculated on the basis of the crystal structures from the observed $D(r) - 4\pi r^2\rho_0$ (the dotted line, as described in a previous section). As seen, the extracted and calculated intermolecular RDFs are in satisfactory agreement with each other over the whole range $r < 20$ Å, and the $EMI^+\cdots TFSI^-$ and $EMI^+\cdots EMI^+$ interactions are clearly observed at around 6 and 9 Å. According to Deetlefs et al.,[10] the DMI^+TFSI^- shows the $DMI^+\cdots TFSI^-$ and $DMI^+\cdots DMI^+$ interactions at around 5.2 and 7.0 Å, respectively. The $EMI^+\cdots TFSI^-$ and $EMI^+\cdots EMI^+$ interactions are slightly longer than the $DMI^+\cdots TFSI^-$ and $DMI^+\cdots DMI^+$ interactions, which is expected because the EMI^+ ion involves a bulkier functional group than the DMI^+ ion. As the observed and calculated RDFs are in satisfactory agreement, we might be able to discuss on the liquid structure on the basis of the present MD simulation.

Local Liquid Structure. The local structure of the crystalline EMI^+TFSI^- must be largely modified in the RTIL, because the RTIL simultaneously involves the planar cis and nonplanar staggered conformers of EMI^+ and the C_1 and C_2 conformers of $TFSI^-$ in equilibrium, whereas the crystals involves only the nonplanar staggered and C_1 conformers. Crystallization of the liquid EMI^+TFSI^- is thus accompanied by the conformational change and intermolecular rearrangement. Indeed, an EMI^+TFSI^- glass obtained by quenching the RTIL involves all conformers of the ions.[31] The freezing point of EMI^+TFSI^- (247 K) is significantly low,[13] compared with that of EMI^+Cl^- (360 K).[32] The difference may be ascribed to the conformational change and intermolecular rearrangement of the $TFSI^-$ ion with a large freedom of geometry change, unlike the small and single atomic chloride ion with a specific affinity to form hydrogen bonds.[33]

As already described, the contact $EMI^+\cdots TFSI^-$ ion pairs involve interactions at around 3.5, 4.6, and 5.7 Å. The number of j ions around an i ion within r_0 is calculated as

$$n_{ij}(r) = \int_0^r (N_j/V) g_{ij}(r)\, dr \qquad (8)$$

where N_j and V denote the total number of j ions in a given volume V. The number of $TFSI^-$ ions around the EMI^+ ion within the first coordination sphere can be evaluated using the $g^{EMI-TFSI}(r)$. The number is about four if we take the value of $r = 9$ Å, at which the $g^{EMI-TFSI}(r)$ shows the minimum (Figure 4), and the same applies also for the $TFSI^-$ ion. This can be illustrated by the space distribution function (SDF), which shows the distribution of the center of mass of $TFSI^-$ around the EMI^+ ion, in Chart S1.

As discussed, the contact $EMI^+\cdots TFSI^-$ ion-pair interaction occurs in the range of 3−6 Å, and specific ion-pair interactions appear at 3.5, 4.6, and 5.7 Å, according to the MD simulation. In order to obtain more detailed information on the $EMI^+\cdots TFSI^-$ interactions, we extracted the partial radial distribution functions of the O and F atoms of $TFSI^-$, $g_{Ci,O}(r)$ and $g_{Ci,F}(r)$, respectively, around a given C_i atom within EMI^+. In Figure 6 are shown the $g_{Ci,O}(r)$ around the imidazolium C2, C4, and C5 atoms. Here, in order to take the conformation into account, the $g_{Ci,O}(r)$s are separately extracted for the nonplanar $EMI^+\cdots C_1$ $TFSI^-$, nonplanar $EMI^+\cdots C_2$ $TFSI^-$, planar $EMI^+\cdots C_1$ $TFSI^-$, and planar $EMI^+\cdots C_2$ $TFSI^-$ interactions. As seen, the $g_{Ci,O}(r)$s show peaks at around 3.5 Å for any set of conformers, and the profile of a given C atom appreciably depends on the set of conformers. The peak at 3.5 Å for the C2, C4, and C5 atoms indicates that all of the C atoms are contacted with the O atom within the $-SO_2(CF_3)$ group of $TFSI^-$. Note that the C2···O interaction shows two sharp peaks at around 3.5 and 5.7 Å, together with a deep valley between the two peaks, whereas the C4···O and C5···O interactions show no sharp peak in the range 4−7 Å. The second peak for the C2 atom is ascribed to the noncontacted O atoms within two $-SO_2(CF_3)$ groups of $TFSI^-$. The sharp second peak suggests that $TFSI^-$ ion locates around the C2 atom of EMI^+ at the distance of a given orientation. Unlike the C2···O interaction, the C4···O and C5···O interactions show no sharp second peak and deep valley, suggesting that the $TFSI^-$ ion locates around the C4 and C5 atoms at the distance of various orientations. The corresponding $g_{Ci,F}(r)$ are given in Figure S2. Evidently, the $g_{C2,F}(r)$ shows a distinct peak at around 5.7 Å. The peak may be ascribed to the F atom within the $-SO_2(CF_3)$ groups of $TFSI^-$ interacting with the C2 atom of EMI^+ through the O atom. The peak at around 3.5 Å is weak, which is consistent with the fact that the C2(EMI^+) site strongly interacts with O($TFSI^-$) atoms rather than F($TFSI^-$) atoms. The more detailed atom−atom correlations will be discussed on the basis of MD simulation using flexible EMI^+ and $TFSI^-$ molecules in a following paper.

NMR Chemical Shifts. The ^{13}C NMR shifts of the EMI^+ ion are shown in Figure 7. The ^1H NMR of the EMI^+ ion and the ^{13}C and ^{19}F NMR of the $TFSI^-$ ion are given in Figures S3

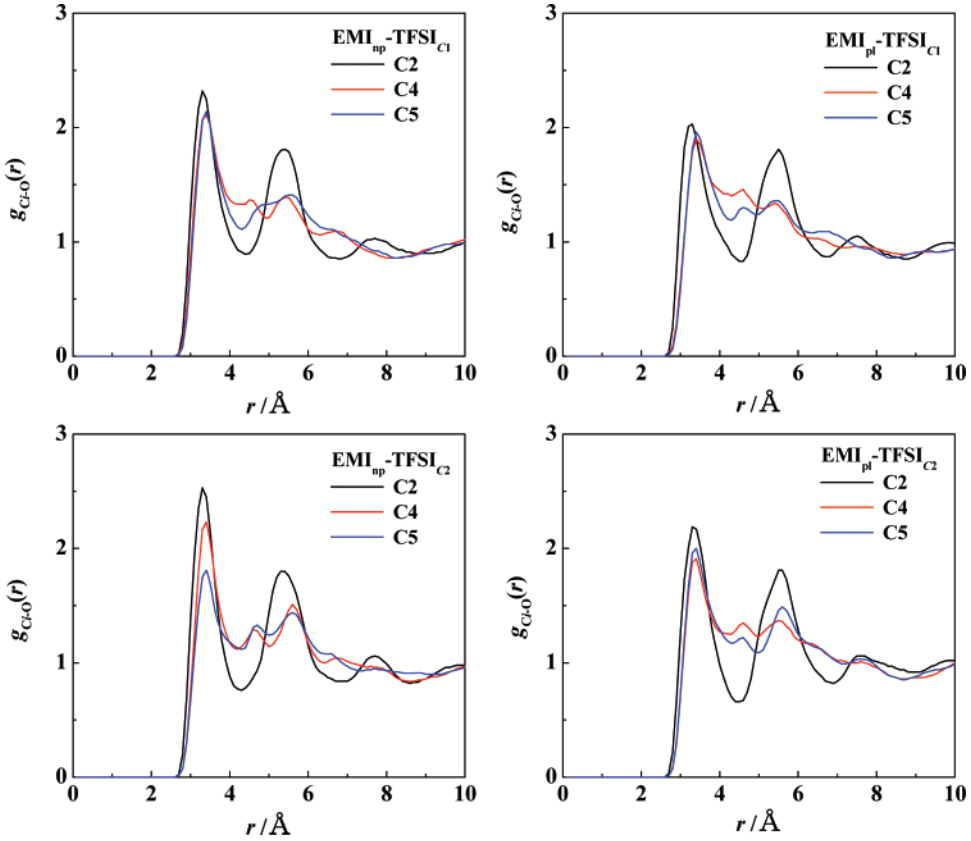

Figure 6. Partial radial distribution functions of the O atom of $TFSI^-$, $g_{Ci,O}(r)$ around the imidazolium C2, C4, and C5 atoms.

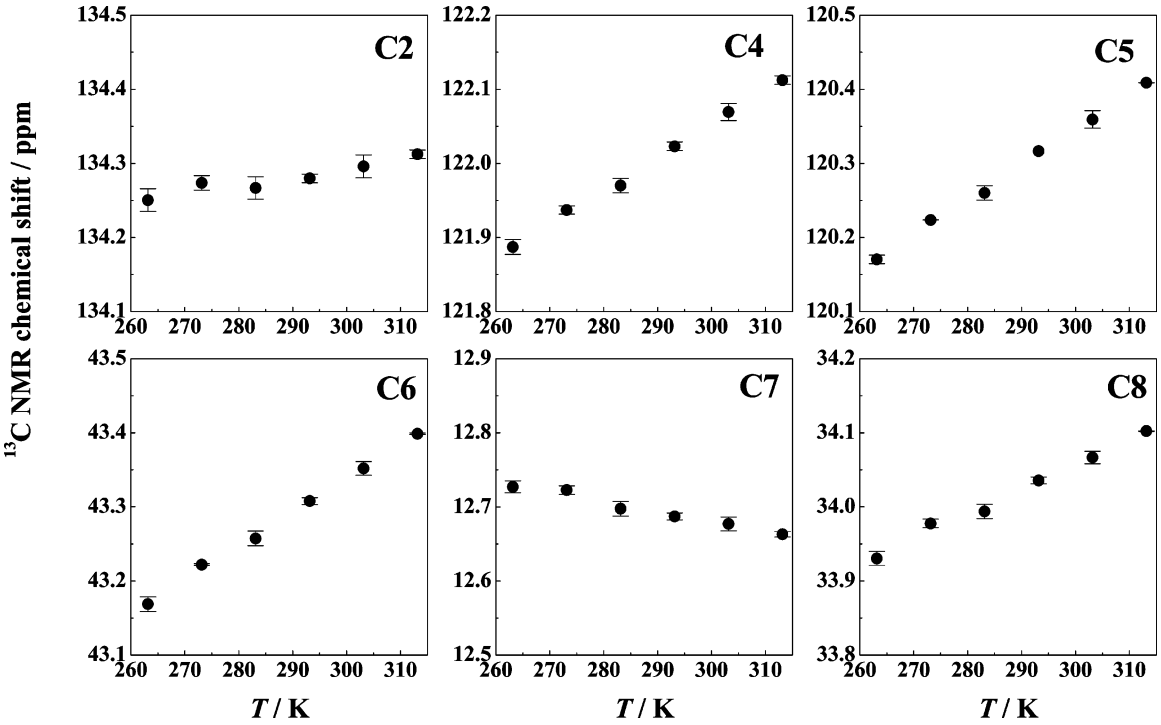

Figure 7. Variation of the ^{13}C NMR chemical shifts with temperature for the C atoms of EMI^+.

and S4. The ^{1}H and ^{13}C NMR signals are assigned according to the literature.[34] The ^{1}H NMR signals monotonically shift to a higher field with increasing temperature, whereas the ^{13}C NMR signals for the C atoms of the imidazolium ring shift to a lower field. These might reflect that the $EMI^+\cdots TFSI^-$ interaction through the −CH proton is weakened with increasing temperature. The relatively strong $-CH\cdots X^-$ hydrogen bonding interaction has been pointed out for the imidazolium C2 proton of the EMI^+ with the anion X^- (X = Cl and PF_6).[33,35] Indeed, the crystal structure indicates that the C2 proton is interacted with two $TFSI^-$ ion through the O atom of the $-SO_2(CF_3)$ group with the $-CH\cdots O$ distance of 3.26−3.30 Å. This might lead to a small shift for the C2 atom relative to that for the C4 or C5 atom. However, according to our MD simulation, the hydrogen bonding interaction is not plausible for the C2 proton. The space distribution functions (SDF) of the O atom of $TFSI^-$

CHART 2: Space Distribution Function (SDF) of the O($TFSI^-$) Atom, Side and Upper Views, around the EMI^+ Conformers

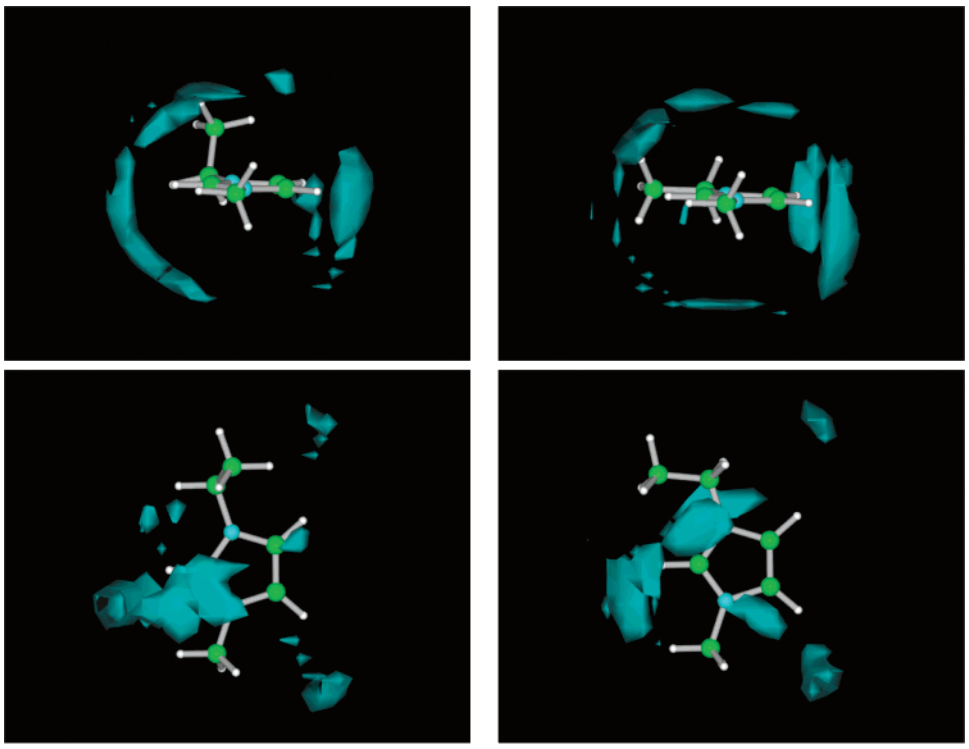

nonplanar staggered EMI^+ **planar cis EMI^+**

around the imidazolium C2 atom are shown in Chart 2. As seen, for both planar cis and nonplanar staggered conformers, the O atoms extensively distribute upper and below the imdazolium ring, and the direction is not limited to that of the favorable −CH···O hydrogen bond. This implies that the charge−charge interaction rather than the hydrogen-bonding interaction plays an essential role for the C2···O interaction. This is recently verified by theoretical calculations for $EMI^+BF_4^-$, according to Tsuzuki.[36] With the terminal C7 atom of the ethyl group of EMI^+, the signal shifts to a higher field with increasing temperature. This is expected, because the ethyl group is not appreciably interacted to change its local position, due to the conformational change of the EMI^+ ion, with increasing temperature. The ^{19}F NMR shows a singlet peak of the CF_3 group at −16.39 ppm at 293 K. Both ^{13}C and ^{19}F NMR of the $TFSI^-$ ion monotonically shift to a lower field with increasing temperature. In crystals, the $-CF_3$ groups from the two parallel layers are contacted through the $-CF_3$···F interactions. The interaction may be weakened or disappeared at an elevated temperature in the liquid state.

Conclusion

The liquid structure of EMI^+TFSI^- RTIL has been studied by LAXS, and the observed RDF was satisfactorily reproduced by the MD simulation over the range $r < 20$ Å. The ionic liquid shows intermolecular interactions at around 6, 9, and 15 Å, which are ascribed to the nearest neighbor EMI^+···$TFSI^-$ interaction, both EMI^+···EMI^+ and $TFSI^-$···$TFSI^-$ interactions, and the second neighbor EMI^+···$TFSI^-$ interaction, respectively. According to the MD simulation, the EMI^+ ion is surrounded by four $TFSI^-$ ions, and vice versa. The imidazolium C2, C4, and C5 atoms of EMI^+ are all mainly contacted with the O atom within the $-SO_2(CF_3)$ group of $TFSI^-$ at around 3.5 Å. This interaction simultaneously brings about the noncontacted interactions of the imidazolium C atoms with the O and F atoms within the $-SO_2(CF_3)$ group at around 5.7 Å. The noncontacted interaction is distinct for the C2 atom, but not for the C4 and C5 atoms, implying that the EMI^+ and $TFSI^-$ ions strongly interact through the C2 atom. This is consistent with the result from NMR. The space distribution of the O($TFSI^-$) atom implies that the charge−charge interaction rather than the hydrogen-bonding interaction plays an essential role for the C2···O interaction. It is shown that the crystal structure of EMI^+TFSI^-, which involves the sole C_1 conformer of $TFSI^-$, is completely destroyed in the RTIL at 298 K.

Acknowledgment. This work has been financially supported by Grants-in-Aid for Scientific Research Nos. 17350037, 18850017, 19003963, 19350033, 19550022, and 19750062 and the Global COE Program "Science for Future Molecular Systems" from the Ministry of Education, Culture, Sports, Science and Technology. The NMR experiments were made at Division of Instrumental Analysis in Analytical Research Center for Experimental Sciences of Saga University.

Supporting Information Available: Space distribution functions (SDF) (Chart S1**)**, calculated $g_i^{EMI-EMI}(r)$s and $g_i^{TFSI-TFSI}(r)$s (Figure S1), partial atom−atom $g^{Ci-F}(r)$s for EMI^+−$TFSI^-$ interactions (Figure S2), variation of the ^1H NMR chemical shifts of EMI^+ and that of the ^{13}C and ^{19}F NMR chemical shifts of $TFSI^-$ with temperature (Figure S3 and S4, respectively). This material is available free of charge via the Internet at http://pubs.acs.org.

References and Notes

(1) Sakaebe, H.; Matsumoto, H. *Electrochem. Commun.* **2003**, *5*, 594.
(2) Garcia, B.; Lavallée, S.; Perron, G.; Michot, C.; Armand, M. *Electrochim. Acta* **2004**, *49*, 4583.
(3) Holzapfel, M.; Jost, C.; Noval, P. *Chem. Commun.* **2004**, 2098.

(4) Seki, S.; Kobayashi, Y.; Miyashiro, H.; Ohno, Y.; Usami, A.; Mita, Y.; Kihira, N.; Watanabe, M.; Terada, N.; *J. Phys. Chem. B* **2006**, *110*, 10228.

(5) (a) Fujii, K.; Kumai, T.; Takamuku, T.; Umebayashi, Y.; Ishiguro, S. *J. Phys. Chem. A* **2006**, *110*, 1798. (b) Fujii, K.; Umebayashi, Y.; Kanzaki, R.; Kobayashi, D.; Matsuura, R.; Ishiguro, S. *J. Solution Chem.* **2005**, *34*, 739. (c) Fujii, K.; Matsumoto, Y.; Kaieda, Y.; Kobayashi, D.; Umebayashi, Y.; Ishiguro, S., *J. Therm. Anal. Cal.* **2006**, *85*, 567−573.

(6) (a) Lopes, J. N. A. C.; Padua, A. A. H. *J. Phys. Chem. B* **2006**, *110*, 3330. (b) Borodin, O.; Smith, G. D., *J. Phys. Chem. B* **2006**, *110*, 11481. (c) Shim, M. Y.; Choi, M. Y.; Kim, H. J, *J. Chem. Phys.* **2005**, *122*, 044511. (d) Liu, Z.; Huang, S.; Wang, W., *J. Phys. Chem. B* **2004**, *108*, 12978.

(7) Takahashi, S.; Suzuya, K.; Kohara, S.; Koura, N.; Curtiss, L. A.; Saboungi, M.-L. *Z. Phys. Chem.* **1999**, *209*, S 209.

(8) Katayanagi, H.; Hayashi, S.; Hamaguchi, H.; Nishikawa, K., *Chem. Phys. Lett.* **2004**, *392*, 460.

(9) Fujii, K.; Kanzaki, R.; Takamuku, T.; Fujimori, T.; Umebayashi, Y.; Ishiguro, S. *J. Phys. Chem. B* **2006**, *110*, 8179.

(10) Deetlefs, M.; Hardacre, C.; Nieuwenhuyzen, M.; Padua, A. A. H.; Sheppard, O.; Soper, A. K. *J. Phys. Chem. B* **2006**, *110*, 12055.

(11) Holbrey, J. D.; Reichert, W. M.; Rogers, R. D. *Dalton Trans.* **2004**, 2267.

(12) Umebayashi, Y.; Fujimori, T.; Sukizaki, T.; Asada, M.; Fujii, K.; Kanzaki, R.; Ishiguro, S. *J. Phys. Chem. A* **2005**, *109*, 8976.

(13) Choudhury, A. R.; Winterton, N.; Steiner, A.; Cooper, A. I.; Johnson, K. A. *CrystEngComm* **2006**, *8*, 742.

(14) Yamanaka, K.; Yamaguchi, T.; Wakita, H. *J. Chem. Phys.* **1994**, *101*, 9830.

(15) Ihara, M.; Yamaguchi, T.; Wakita, H.; Matsumoto, T. *Adv. X-ray Anal. Jpn.* **1994**, *25*, 49.

(16) Furukawa, K. *Rep. Progr. Phys.* **1962**, *25*, 395.

(17) Krogh-Moe, J. *Acta Crystallogr.* **1956**, *2*, 951.

(18) Norman, N. *Acta Crystallogr.* **1957**, *10*, 370.

(19) (a) Cormer, D. T.; Mann, J. B. *J. Chem. Phys.* **1967**, *47*, 1892. (b) Cromer, D. T. *J. Chem. Phys.* **1969**, *50*, 4857.

(20) Maslen, E. N.; Fox, A. G.; O'Keefe, M. A. *International Tables For Crystallography*; Kluwer: Dorfrecht, 1999; Vol. C, pp 572−574.

(21) Johanson, G.; Sandstörm, M., *Chem. Scr.* **1973**, 4, 195.

(22) (a) Lopes, J. N. C.; Deschamps, J.; Padua, A. A. H. *J. Phys. Chem. B* **2004**, *108*, 2038. (b) Lopes, J. N. C.; Deschamps, J.; Padua, A. A. H. *J. Phys. Chem. B* **2004**, *108*, 11250.

(23) Lopes, J. N. C.; Padua, A. A. H. *J. Phys. Chem. B* **2004**, *108*, 16893.

(24) Mizuno, K.; Imafuji, S.; Ochi, T.; Ohta, T.; Maeda, S. *J. Phys Chem. B* **2000**, *104*, 11001.

(25) Momoki, K.; Fukazawa, Y. *Anal. Chem.* **1990**, *62*, 1665.

(26) Momoki, K.; Fukazawa, Y. *Anal. Sci.* **1994**, *10*, 53.

(27) Mukhomorv, R. V. K. *Zh. Fizch. Khim.* **1986**, *60*, 360.

(28) Matusmoto, K.; Tsuda, T.; Hagiwara, R.; Ito, Y.; Tamada, O. *Solid State Sci.* **2002**, *4*, 23.

(29) Choudhury, A. R.; Winterton, N.; Steiner, A.; Cooper, A. I.; Johnson, K. A. *J. Am. Chem. Soc.* **2005**, *127*, 16792.

(30) Fujii, K.; Seki, S.; Fukuda, S.; Kanzaki, R.; Takamuku, T.; Umebayashi, Y.; Ishiguro, S. *J. Phys. Chem. B*, in press.

(31) Lassègues, J. C.; Grondin, J.; Holomb, R.; Johansson, P. *J. Raman Spec.* **2007**, *38*, 551.

(32) Wasserscheid, L. P.; Welton, T. *Ionic Liquids in Synthesis*; Wiley-VCH: Weinheim, Germany, 2003.

(33) Hardacre, C.; Holbrey, J. D.; McMath, S. E. J.; Brown, D. T.; Soper, A. K. *J. Chem. Phys.* **2003**, *118*, 273.

(34) Su, B.-M.; Zhang, Z. C. *J. Phys Chem. B* **2004**, *108*, 19510.

(35) Hardacre, C; McMath, S. E. J.; Nieuwenhuyzen, M.; Bowron, D. T.; Soper, A. K. *J. Phys.: Condens. Matter* **2003**, *15*, S159.

(36) Tsuzuki, S.; Tokuda, H.; Mikami, M. *Phys. Chem. Chem. Phys.* **2007**, *9*, 4780.